Theoretical & Applied Mechanics Letters 8 (2018) 272-276

Contents lists available at ScienceDirect

Theoretical & Applied Mechanics Letters

journal homepage: www.elsevier.com/locate/taml

Letter

Dynamic rupture of metal sheet subjected to laser irradiation and tangential subsonic airflow

Xiaodong Xing[a], Te Ma[a,b], Ruixing Wang[b,c], Chenyu Cao[a,b], Hongwei Song[b,c,*], Chenguang Huang[b,c]

[a] *Harbin Engineering University, Harbin 150000, China*
[b] *Key Laboratory for Mechanics in Fluid-Solid Coupling Systems, Institute of Mechanics, Chinese Academy of Sciences, Beijing 100190, China*
[c] *School of Engineering Science, University of Chinese Academy of Sciences, Beijing 100049, China*

ARTICLE INFO

Article history:
Received 18 May 2018
Received in revised form 9 June 2018
Accepted 11 June 2018
Available online 25 June 2018

Keywords:
Thermal-fluid-structure coupling
Thermal elastoplastic
Aerodynamic pressure
Laser damage
Dynamic rupture

ABSTRACT

To reproduce the premature rupture process of metal sheet subjected to laser irradiation with subsonic airflow, which is an interesting phenomenon observed in the experiments given by Lawrence Livermore National Laboratory, a coupled numerical model considering the interaction and evolution of metal elastoplastic deformation and aerodynamic pressure profile is presented. With the thermal elastoplastic constitutive relationship and failure criterion, the simulated failure modes and dynamic rupture process are basically consistent with the experimental results, indicating plastic flow and multiple fracturing is the main failure mechanism. Compared with the case of non-airflow, subsonic airflow not only accelerates deformation, but also turns the bugle deformation, plastic strain and rupture mode into asymmetric.

The presence of tangential airflow may significantly change the behavior of laser interaction with materials due to the effects of shear force, oxygen supply and forced convection [1-9]. For instance, the airflow may blow away the melted metal or pyrolytical products, enhance the oxidation or combustion process, resulting in an accelerated ablation rate and a reduced burn-through time. Recently a new effect due to airflow observed by Lawrence Livermore National Laboratory has drawn much attention [10]. When high power laser irradiated a thin aluminum sheet subjected to subsonic airflow, the target ruptures at the temperature well below the melting point. This result is different from the melting damage under a non-airflow condition. They summarized this is due to the aerodynamic effect: airflow decreases the pressure on the side of the incident beam by $p = 1/2\rho v^2$. They further gave a quantitative analysis of the bulge deformation due to the combining effects of material softening and pressure difference, based on an elastic model [10].

However, the essence of this case is a complex physical process including elastic bulging, plastic flow, and multiple fracturing. The elastic model can reasonably predict the bulge deformation profile, however it is not enough to capture the complete physical mechanism. Up to now no relevant work has been reported to reproduce this dynamic rupture process through a rigorous model. To reach this goal, two important steps are adopted in our case. Firstly, a coupled thermal-fluid -structure model considering the interaction of laser source, thin aluminum sheet and subsonic tangential airflow should be built [11-14]. The coupling thermal/mechanical loads induced by laser source and aerodynamic pressure decrease should be exerted to the thin target, and the influence of the thin target deformation to the airflow pattern and aerodynamic pressure should be recalculated before next time-step exertion. Similar approach has been reported by Huang et al. [15] and Song and Huang [16], when they investigated the influence of supersonic airflow on the development of laser ablation pit. Secondly, to verify that plastic flow and multiple fracturing is the main damage mechanism, a thermal elastoplastic constitutive relationship [17, 18] and failure criterion should be incorporated in the numerical model.

* Corresponding author.
E-mail address: songhw@imech.ac.cn (H.W. Song).

http://dx.doi.org/10.1016/j.taml.2018.04.003

In the experiment, the pulsed solid-state laser equivalent to a continuous wave (CW) laser with an average power of 25 kW is employed. The size of laser beam is 0.13×0.13 m^2, and the aluminum plate target is $0.4 \times 0.4 \times 0.0018$ m^3. On the laser irradiation side, tangential airflow with a constant velocity of 100 m/s is produced by the blowing device and the suction device. According to Bernoulli's law, the wind stream produces a pressure decrease near the airflow surface of aluminum sheet by $\Delta p = p_a - p_s = 1/2\rho v^2$, where v is local airflow velocity, ρ is gas density, where p_a is atmospheric pressure, p_s is surface pressure. In the light of Fig. 1, the pressure difference is not constant across the target. In the center of laser beam, the bulge deformation and airflow velocity v_1 are the highest, therefore the aerodynamic pressure decrease $\Delta p_1 = p_a - p_{s1}$ is the largest. The instantaneous local deformation, airflow velocity and pressure difference at moments before rupture initiation are coupled together, and should be determined by the coupled numerical model.

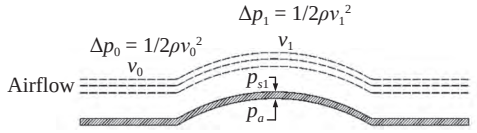

Fig. 1. Physical model of local deformation, airflow velocity and pressure difference.

The bugle deformation and dynamic rupture behavior are simulated by finite element analysis (FEA) with an Abaqus code, and the airflow characteristics and aerodynamic effects are simulated computation fluid dynamics (CFD) with a Fluent code. In the coupled fluid-structure analysis, the CFD transfers instantaneous pressure decrease produced by tangential airflow to the FEA through the controlling interface, and the FEA transfers the instantaneous target deformation morphology to CFD. The staggered iteration and data exchange continues until element crack initiation in the FEA.

In the FEA, the essence of the target failure process is thermal elastoplastic deformation and dynamic rupture, which is related to the problems of heat transfer, physical non-linearity and geometrical non-linearity. Thermal boundary condition in the laser irradiation region is

$$-k\frac{\partial T}{\partial n} = q_{\text{laser}} + h(T_{\text{w}} - T_\infty) + \varepsilon\sigma T_{\text{w}}^4, \quad (1)$$

where k is thermal conductivity, $\dfrac{\partial T}{\partial n}$ is temperature gradient, q_{laser} is the absorbed laser heat flux, h is convective heat transfer coefficient, T_{w} is the surface wall temperature, T_∞ is environment temperature, ε is emissivity, σ is Stefan-Boltzmann constant. The heat flux due to the forced convection and thermal radiation is negligible compared to heat flux of laser source (10^4 W/m^2 vs. 10^6 W/m^2). The laser absorption coefficient 0.75 is adopted.

The effect of thermal softening on the mechanical strength of materials should be considered. Elastoplastic constitutive model of material is employed

$$\sigma_{ij} = \lambda(\varepsilon_{kk} - \varepsilon_{kk}^p)\delta_{ij} + 2G(\varepsilon_{ij} - \varepsilon_{ij}^p) - \frac{E}{1-2\nu}\alpha(T - T_0)\delta_{ij}, \quad (2)$$

where λ and G are Lame constants, which can be obtained by Young's modulus and Poisson's ratio, E is Young's modulus, ν is Poisson's ratio, α is coefficient of linear expansion, ε_{ij}^p is plastic strain tensor, T_0 is initial temperature. In the analysis the bilinear isotropic hardening model is employed. The thermal properties of the target material are listed in Table 1, where T is temperature, C is specific heat capacity, σ_s is yield strength, σ_b is tensile strength. And the failure mode of the target is simulated by element damage failure method, and the failure criterion is the maximum equivalent plastic strain.

Figure 2 gives the comparison of dynamic rupture process between experimental and numerical results. The figure includes information of rupture mode, maximum temperature and time sequence. It can be seen that the numerical model basically reproduced this premature failure process before melting point. The rupture process last from 1.71 s to 2.28 s with the maximum temperature ranging from 683 K to 800 K in the numerical simulation, where it is from 1.73 s to 2.40 s with the maximum temperature from 683 K to 795 K in the experiment. At about 1.7 s, multiple cracks initiated. Under the combined effects of thermal softening and aerodynamic pressure, multiple local plastic strains reached the failure value in the thin aluminum sheet. The numerical modeling confirms that the main failure mechanism is plastic flow and fracture. As cracks propagation and convergence, multiple debris formed and removed from the target, leaving a hole in the laser irradiated area. The numerically simulated fracture mechanism and final damage morphology is resemble to that of experiment, as can be found in Figs. 2 and 4 in Ref. [10].

In order to give a detailed description of the effect of tangential airflow on the target, we give the characteristics of the airflow at t=1.7 s, which is the moment right before rupture crack initiation, as illustrated in Fig. 3. According to Fig. 3(a), when the airflow passes through the bugled aluminum sheet, the velocity increases in the convex ridge of the bulge to a maximum value of 115 m/s, whereas it decreases at the foot of the bugle to a minim-

Table 1 Thermal-mechanical parameters of aluminum alloy versus temperature

T (K)	k(W·m^{-1}·K^{-1})	C (J·kg^{-1}·K^{-1})	α(10^{-6} K^{-1})	E (GPa)	σ_s(MPa)	σ_b(MPa)
293	155	900	21.4	68	411	638
373	159	921	23.1	64	396	580
473	163	1047	25.2	54	274	399
573	163	1130	26.8	42	161	178
673	159	1172	28.4	29	67	68

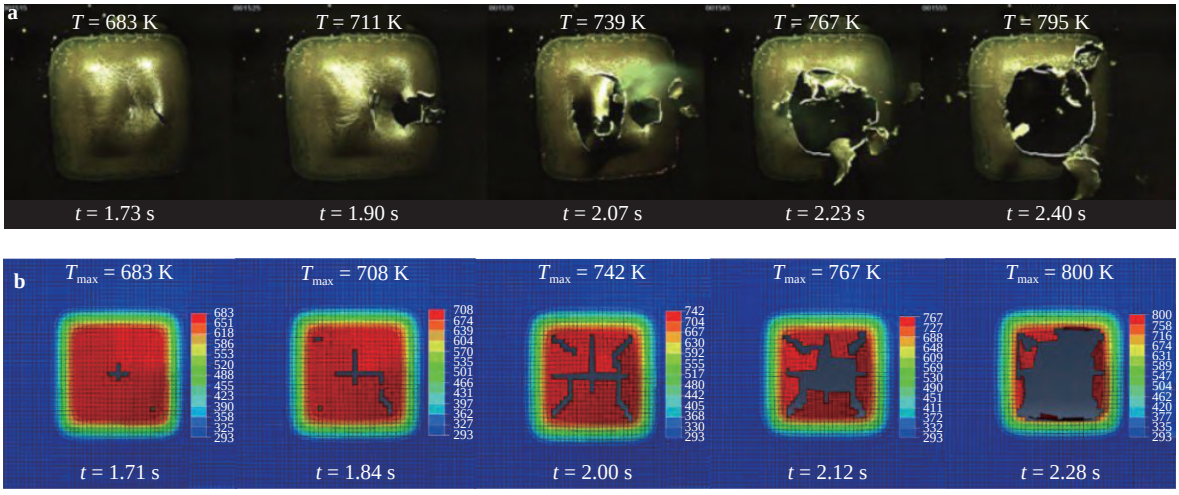

Fig. 2. Comparison of dynamic rupture process. **a** Experiment [10]. **b** Numerical simulation.

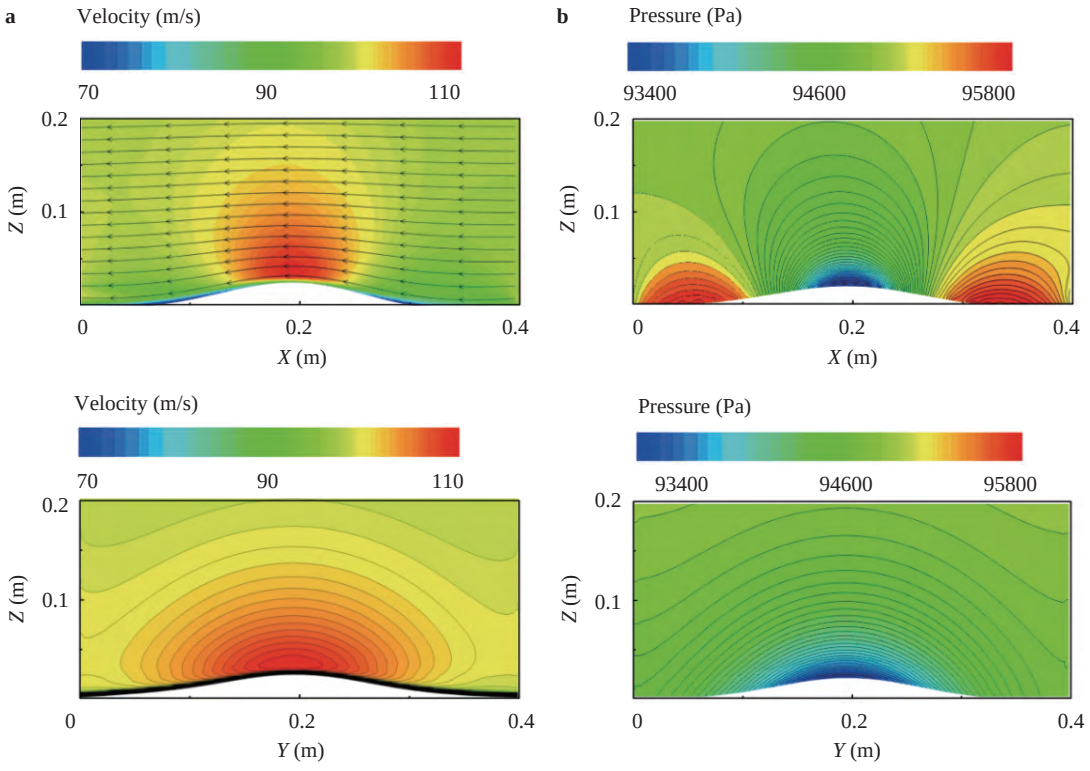

um value of 70 m/s in the airflow direction (top figure). However, velocity profile in the cross-section of airflow demonstrate only high values, typically larger than initial airflow velocity of 100 m/s (bottom figure). This results in different pressure profiles when viewing from two cross-sections. As can be seen from Fig. 3(b), the dimension of the low pressure region in the airflow direction is smaller than the laser irradiation region (top figure), whereas it is slightly larger than laser spot in the cross-section of airflow (bottom figure). This is the reason why most cracks propagate perpendicular to the airflow direction, as can be found in the first three frames both of the experiment and numerical simulation in Fig. 2. According to the above results, we can better grasp the failure process of aluminum sheet. The first crack appears near the center of the target, then multiple cracks are initiated and propagate along the direction perpendicular to airflow, due to the asymmetric pressure distribution.

We have also simulated the case of laser irradiation without airflow. Comparison of deformation and equivalent plastic strain on the transverse and longitudinal lines at the center of the laser spot for the cases with airflow and without airflow is shown in Fig. 4. This figure also includes information of aerodynamic pressure evolution and bulge deformation evolution with irradi-

ation time, see Fig. 4(a) and 4(b). In the early stage of laser irradiation, the tangential airflow has little influence on the deformation of the target since the temperature is relatively low, e.g., 1 s in Fig. 4(b). When the aluminum sheet is heated up to 650 K, thermal softening effect becomes dominant and the strength nearly vanishes. Meanwhile, with the increase of bugle deformation, the local airflow velocity near the sheet surface accelerates, resulting an increase of aerodynamic pressure difference. At the

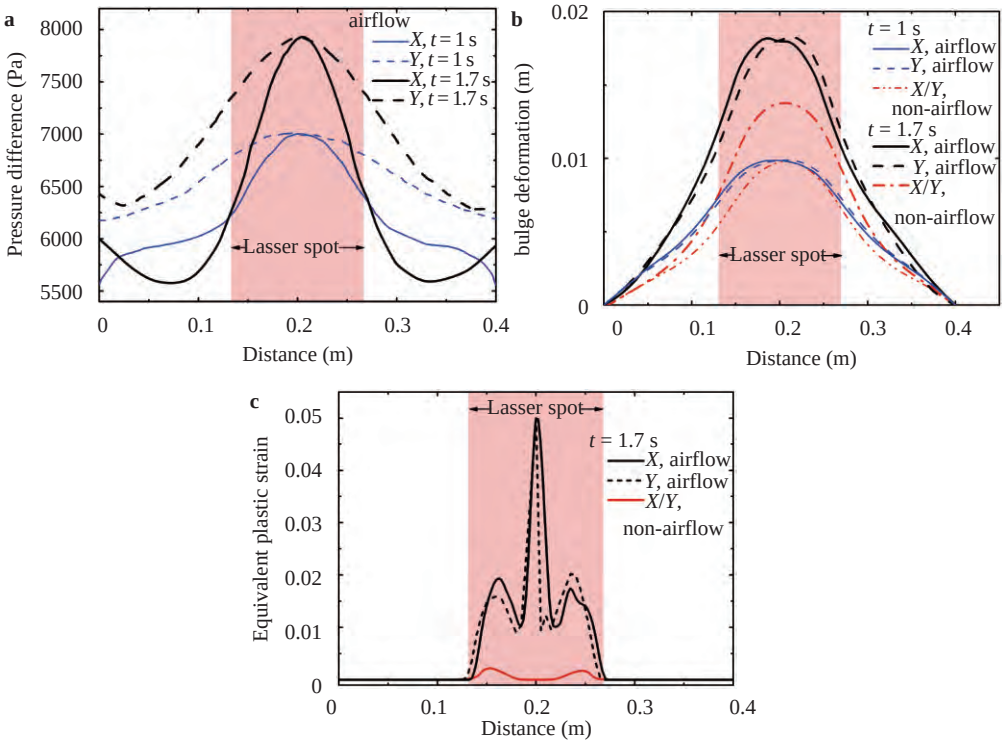

Fig. 4. The effect of airflow on target (*X* is along airflow view, *Y* is cross-section view of airflow). **a** Aerodynamic pressure difference. **b** Deforma-

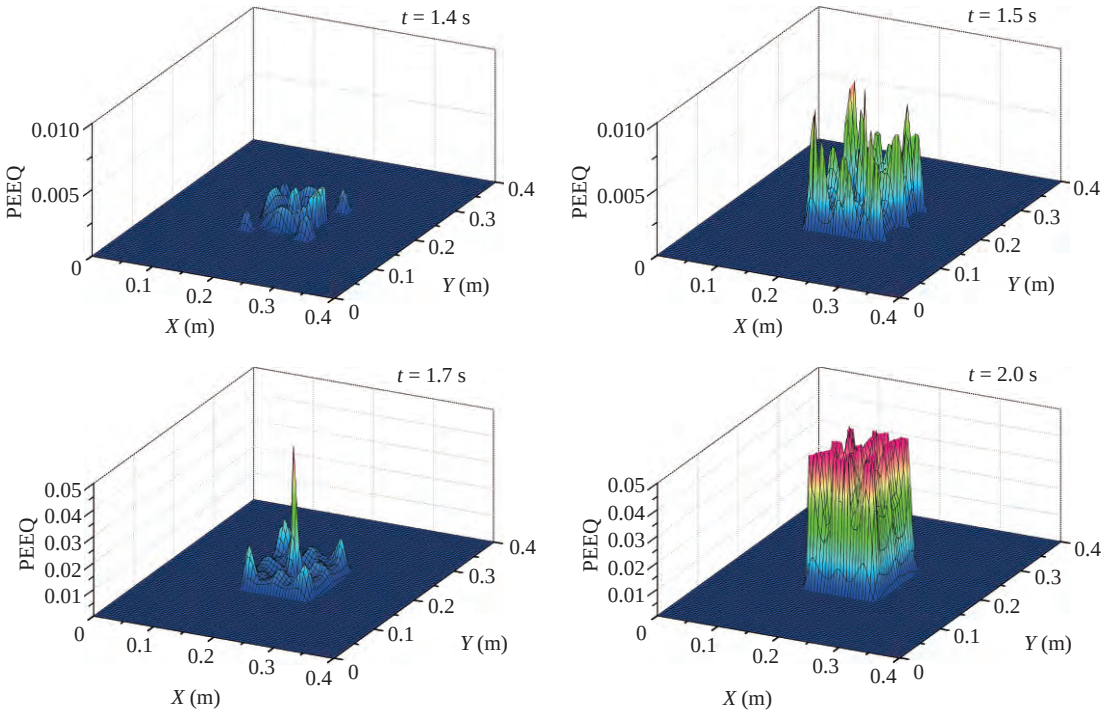

Fig. 5. Evolution of equivalent plastic strain (PEEQ).

1.7 s moment, the largest deformation is 0.0183 m and 0.0137 m for airflow condition and non-airflow condition, respectively. In contrast, the largest deformation given by elastic model is 0.0153 m [10], which is about 16.4% error from the elastoplastic model and coupling analysis. Meanwhile, in the case of non-airflow the deformation field is symmetric, whereas the aerodynamic force breaks this symmetry. In Fig. 4(c), the equivalent plastic strain in an airflow case shows a main peak at the center of the laser spot, so the first crack typically appears here. It also has two sub-peak areas, which can explain the multiple cracks formed around the center in the subsequent time step. In a non-airflow case, the equivalent plastic strain is very low. At the 1.7 s moment, the target is far from the fracture condition, and it will fail in the form of melting later on.

Figure 5 gives the evolution of equivalent plastic strain from 1.4 s to 2.0 s. The plastic strain increased significantly during this period, mainly due the rapid increase in target temperature. The temperature at 1.4 s is 616 K, where as at 1.7 s is 681 K. According to Table 1, the elastic modulus drops from 42 GPa to 29 GPa when temperature rise from 573 K to 673 K. The coupled effects of material softening, bugle deformation and aerodynamic pressure lead to a rapid failure in this period.

In summary, we have proposed a coupled thermal-fluid-structure model include thermal elastoplastic constitutive relationship to investigate the coupled deformation and dynamic failure process of laser irradiated metal sheet under the tangential subsonic airflow. The behavior of target rupture at the temperature well below the melting point induced by the thermal softening and aerodynamic pressure decrease is reproduced, and the mechanisms of multiple cracks initiation is revealed. It is found that plastic flow and multiple fracturing is the main failure mechanism, and the nonlinear elastoplastic constitutive relationship of the material must be considered. The coupled analysis with thermal elastoplastic bugle deformation is 16.4% larger in comparison with the decoupled elastic model. Compared with the case of non-airflow, subsonic airflow enlarges the bugle deformation from 0.0137 m to 0.0183 m, which is about 33.6% increase. Meanwhile, it turns the bugle deformation, plastic strain and rupture mode into asymmetric.

Acknowledgements

This research is supported by the National Natural Science Foundation of China (11472276, 11332011, and 11502268) and the National Defense Basic Scientific Research Program of China (JCKY2016130B009).

References

[1] H.N. Jia, X.J. Yang, W. Zhao, et al., Femtosecond laser pulses for drilling the shaped micro-hole of turbine blades, Chin. Phys. Lett. 30 (2013) 044202.

[2] C.W. Wu, C.G. Huang, G.N. Chen, et al., Laser heating induced plastic deformation in a pre-elastic-stretched titanium alloy strip, Opt. Laser. Technol 45 (2013) 558–564.

[3] K.H. Leitz, H. Koch, A. Otto, Numerical simulation of process dynamics during laser beam drilling with short pulses, Appl. Phys. A. 106 (2012) 885–891.

[4] P. Hu, F.L. Chen, Numerical simulation of plane target in airflow under laser irradiation, High Power Laser and Particle Beams 23 (2011) 1935–1939. (in Chinese)

[5] J. Zhang, C.G. Huang, Numerical simulation of airflow effect on moving body under laser irradiation, High Power Laser and Particle Beams 19 (2007) 1817–1821. (in Chinese)

[6] F.J. Gürtler, M. Karg, K.-H. Leitz, et al., Simulation of laser beam melting of steel powders using the three-dimensional volume of fluid method, Phys. Procedia 41 (2013) 881–886.

[7] K. Abderrazak, W. Kriaa, W.B. Salem, et al., Numerical and experimental studies of molten pool formation during an interaction of a pulse laser (Nd:YAG) with a magnesium alloy, Opt. Laser. Thchnol 41 (2009) 470–480.

[8] E.D. Cabanillas, M.F. Creus, R.C. Mercader, Microscopic spheroidal particles obtained by laser cutting, J. Mater. Sci. 40 (2005) 519–522.

[9] O.U. Khan, B.S. Yilbas, Laser heating of sheet metal and thermal stress development, J. Mater. Process. Tech. 155 (2004) 2045–2050.

[10] C.D. Boley, K.P. Cutter, S.N. Fochs, Interaction of a high-power laser beam with metal sheets, J. Appl. Phys. 107 (2010) 043106.

[11] D.B. Aukje, B. Hester, V.Z. Alexander, Comparing different methods for the coupling of non-matching meshes in Fluid-Structure Interaction computations, AIAA CFD Conference, Toronto, 2005

[12] W. Dettmer, D.A. Peri, A computational framework for fluid-structure interaction: finite element formulation and applications, Comp. Meth. Appl. Mech. Eng. 195 (2006) 5754–5779.

[13] B. Hassan, D.W. Kuntz, D.E. Salguero, et al., A coupled fluid/thermal/flight dynamics approach for predicting hypersonic vehicle performance, AIAA Paper (2001) 2903

[14] M.S. Holden, T.P. Wadhams, G.J. Smolinski, et al., Experimental and numerical studies on hypersonic vehicle performance in the LENS shock and expansion tunnels, AIAA paper (2006) 125

[15] Y.H. Huang, H.W. Song, C.G. Huang, Heat transfer and mode transition for laser ablation subjected to supersonic airflow, Chin. Phys. Lett. 33 (2015) 014201.

[16] H.W. Song, C.G. Huang, Progress in thermal-mechanical effects induced by laser, Adv. Mech. 46 (2016) 201610.

[17] X.L. Tian, A.B. Yu, A thermal elastoplastic model of the surface residual stress of ceramics grinding, J. Mater. Process. Tech. 129 (2002) 451–453.

[18] N. Isao, O. Jun-ichiro, K.Ryoichi, A simulation analysis on the thermal elastoplastic deformation of steel plate by high frequency induction heating, J. Soc. Naval Arch. Jap. 174 (1993) 535–542.